Magnetohydrodynamic simulation of the interaction between two interplanetary magnetic clouds and its consequent geoeffectiveness: 2. Oblique collision

Ming Xiong,[1] Huinan Zheng,[1] and Shui Wang[1]

[1]   The numerical studies of the interplanetary coupling between multiple magnetic clouds (MCs) are continued by a 2.5-dimensional ideal magnetohydrodynamic (MHD) model in the heliospheric meridional plane. The interplanetary direct collision (DC)/oblique collision (OC) between both MCs results from their same/different initial propagation orientations. Here the OC is explored in contrast to the results of the DC. Both the slow MC1 and fast MC2 are consequently injected from the different heliospheric latitudes to form a compound stream during the interplanetary propagation. The MC1 and MC2 undergo contrary deflections during the process of oblique collision. Their deflection angles of $|\delta\theta_1|$ and $|\delta\theta_2|$ continuously increase until both MC-driven shock fronts are merged into a stronger compound one. The $|\delta\theta_1|$, $|\delta\theta_2|$, and total deflection angle $\Delta\theta$ ($\Delta\theta = |\delta\theta_1| + |\delta\theta_2|$) reach their corresponding maxima when the initial eruptions of both MCs are at an appropriate angular difference. Moreover, with the increase of MC2's initial speed, the OC becomes more intense, and the enhancement of $\delta\theta_1$ is much more sensitive to $\delta\theta_2$. The $|\delta\theta_1|$ is generally far less than the $|\delta\theta_2|$, and the unusual case of $|\delta\theta_1| \simeq |\delta\theta_2|$ only occurs for an extremely violent OC. But because of the elasticity of the MC body to buffer the collision, this deflection would gradually approach an asymptotic degree. As a result, the opposite deflection between the two MCs, together with the inherent magnetic elasticity of each MC, could efficiently relieve the external compression for the OC in the interplanetary space. Such a deflection effect for the OC case is essentially absent for the DC case. Therefore, besides the magnetic elasticity, magnetic helicity, and reciprocal compression, the deflection due to the OC should be considered for the evolution and ensuing geoeffectiveness of interplanetary interaction among successive coronal mass ejections.

1.   Introduction

[2]   One of the greatest concerns within the current space science community has been increasingly focused on the Sun-Earth system, which is intimately linked by the solar wind. The solar wind originates from the chromospheric network [*Xia et al.*, 2003; *Xia*, 2003; *Xia et al.*, 2004], according to the measurements of ultraviolet emission and Doppler shifting speed in the inner corona, carries non-Wentzel-Kramers-Brillouin Alfvén Waves in the differential flow of multiple ion species [*Li and Li*, 2007,

2008], is very likely driven by an ion cyclotron resonance mechanism via the Kolmogorov turbulent cascade [*Li et al.*, 2004], and transports the angular momentum from the Sun [*Li and Li*, 2006; *Li et al.*, 2007; *Li and Li*, 2009]. The ubiquitous interplanetary solar wind highly fluctuates, owing to outward emanating disturbances from solar activities. Therefore, the Sun serves as the driver for the cause-and-effect transporting chain of space weather.

[3]   The interplanetary space, which *Dryer* [1994] called a "transmission channel" between the Sun and the Earth, is a nonlinear system consisting of various discontinuous fronts, diffusion processes, and couplings between different spatial and temporal scales. A magnetic flux rope levitating in the corona may suddenly lose its equilibrium and consequently escape into the interplanetary space [*Chen et al.*, 2006, 2007]. The interplanetary manifestation of such a magnetic rope is identified as a magnetic cloud (MC) with enhanced magnetic field magnitude, smooth rotation of the magnetic

---

[1]Chinese Academy of Sciences Key Laboratory for Basic Plasma Physics, School of Earth and Space Sciences, University of Science and Technology of China, Hefei, China.

field vector, and low proton temperature [*Burlaga et al.*, 1981]. The passage of an MC across the Earth triggers a significant geomagnetic storm because of large southward magnetic flux in the MC body [*Tsurutani et al.*, 1988; *Gosling et al.*, 1991]. Hence MCs are an important subset of interplanetary coronal mass ejections (ICMEs), whose fraction is ~100%, though with low statistics, at solar minimum and ~15% at solar maximum [*Richardson and Cane*, 2004]. Especially at solar maximum, when the daily occurrence rate of CMEs is about 4.3 on average based on the SOHO/Lasco CME catalogue (http://cdaw.gsfc.nasa. gov/CME_list), CMEs very likely interact with each other on their journey toward the Earth. Two distinct observation events of interaction between an early slow CME1 and a late fast CME2 within 30 solar radii were presented by *Gopalswamy* [2002]: (1) two fast CMEs on 4 November 1997, which were initially 100° apart in relation to their source regions according to Yohkoh/SXT observation, led to the plowing of the CME2-driven shock through the CME1 in the field of view (FOV) of Lasco C2/C3; (2) two fast CMEs from the same source region on 20 January 2001, initially two hours apart, were later indistinguishable in the FOV of Lasco C3, and are therefore thought to have cannibalized each other. As the coupling of multiple CMEs from the same/different heliographic location of source region is defined as the direct collision (DC)/oblique collision (OC) by *Xiong et al.* [2006b], these two events of 4 November 1997 and 20 January 2001 are the cases of OC and DC, respectively. The radio signatures of CME cannibalism typically precede the intersection of the leading edge trajectories and behave as an intense continuum-like radio emission enhancement, usually following a type II radio burst on basis of Wind/WAVES observation [*Gopalswamy et al.*, 2001, 2002]. *Gopalswamy et al.* [2002] argued that the nonthermal electrons responsible for this new type of ratio emission are accelerated because of magnetic reconnection between two CMEs and/or the formation of a new shock at the time of collision between two CMEs. Meanwhile, some interplanetary complicated structures were also reported in the near-Earth space, such as the complex ejecta [*Burlaga et al.*, 2002], compound stream [*Burlaga et al.*, 1987; *Wang et al.*, 2003a; *Dasso et al.*, 2009], shock-penetrated MCs [*Lepping et al.*, 1997; *Wang et al.*, 2003b; *Berdichevsky et al.*, 2005], and non-pressure-balanced "MC boundary layers" associated with magnetic reconnection [*Wei et al.*, 2003, 2006]. According to the in situ observations of spacecraft at 1 AU, the evolutionary signatures of ICMEs' interaction include heating of the plasma, acceleration/deceleration of the leading/trailing ejecta, compressed field and plasma in the leading ejecta, possible disappearance of shocks, and strengthening of the shock driven by the accelerated ejecta [*Farrugia and Berdichevsky*, 2004]. Since magnetic diffusion in the interplanetary space is much less than that in the solar corona, the cannibalism of CMEs that interact in the Lasco FOV [*Gopalswamy et al.*, 2001, 2002] should not occur in the interplanetary space [*Xiong et al.*, 2007]. Moreover, formed by multiple CMEs/ICMEs colliding, the compound stream at 1 AU could be in a different evolutionary stage. The position of the overtaking shock at 1 AU can be (1) still in the MC, such as an 18 October 1995 event [*Lepping et al.*, 1997] and a 5–7 November

2001 event [*Wang et al.*, 2003b], or (2) ahead of the MC after ultimately penetrating it [*Berdichevsky et al.*, 2005]. The compressed magnetic field downstream of the shock front is northward for the 18 October 1995 event [*Lepping et al.*, 1997] and southward for the 5–7 November 2001 event [*Wang et al.*, 2003b]. Therefore, the latter event of 5–7 November 2001 resulted in a great magnetic storm of $Dst \approx -300$ nT. An important interplanetary origin for the great geomagnetic storms have already been identified by the observations [*Wang et al.*, 2003a; *Farrugia et al.*, 2006; *Dasso et al.*, 2009] and simulations [*Xiong et al.*, 2006a, 2006b, 2007; *Xiong*, 2007] as multi-ICME structures, accompanying intense compression of southward magnetic flux during the interaction process. When the compound structure reaches the Earth through the interplanetary space, its physical parameters are jointly decided by three factors: (1) individual CMEs themselves, (2) inhomogeneous interplanetary medium, and (3) irreversible interacting process among these CMEs/ICMEs [*Xiong*, 2007]. Because of the intractability of analytical reduction, compound structures resulting from the interaction of multiple CMEs/ICMEs have been extensively studied in numerical simulations: e.g., complex ejecta [*Xiong et al.*, 2005], interaction of a shock wave with an MC [*Vandas et al.*, 1997; *Xiong et al.*, 2006a, 2006b], and coupling of multiple MCs [*Schmidt and Cargill*, 2004; *Lugaz et al.*, 2005; *Xiong et al.*, 2007]. Particularly, *Xiong et al.* [2005, 2006a, 2006b, 2007] and *Xiong* [2007] conducted a systematic and delicate numerical MHD simulation of interplanetary compound structures in terms of their formation, propagation, evolution, and ensuing geoeffectiveness. These simulation works do well provide theoretical interpretations for physical phenomena of compound structures observed by the SOHO, Wind, and ACE spacecraft.

[4] The radial liftoff of a CME at its onset phase from a solar source region sometimes deviates from the radial ray during its outward movement. The nonstraight trajectory substantiates that deflections do happen during CME/ICME propagation. The deflection effect plays a notable role in space weather predicting, since the first step of prediction is whether or not a solar eruption will ultimately affect the geospace environment [*Williamson et al.*, 2001]. The near-Sun trajectory of a CME can be directly imaged by remote sensing of a white light coronagraph on board such spacecraft as Skylab, SOHO, and STEREO. *MacQueen et al.* [1986] found that 29 CME events observed during the Skylab epoch of solar minimum from 1973 to 1974 underwent an average 2.2° equatorward deflection, and ascribed the deflection to the nonradial forces arising from the background coronal magnetic and flow patterns. *Cremades and Bothmer* [2004] identified the CME events from the SOHO/Lasco FOV and their corresponding source regions from the SOHO/EIT and SOHO/MDI from January 1996 to December 2002, and found that the position angle (PA) of Lasco-imaged CMEs deviates statistically about 18.6° southward toward the lower latitude at solar minimum. They also ascribed such equatorward deflection of CMEs from solar activity belts to the surrounding fast solar wind from polar coronal holes with a stronger total plasma and magnetic field pressure. *Gopalswamy et al.* [2001] reported that on 10 June 2000, a slow CME of 290 km/s was overtaken by a fast CME of 660 km/s from a different

solar source region; the core of the slow CME was leftward deviated by $13°$ in terms of the PA in the Lasco/C3 FOV. *Zhang et al.* [2004] also reported a nonradial motion of a gradually accelerated CME on 19 October 1997 from the SOHO observation. This peculiar CME was initiated above the east limb at northern latitude $14°N$ in the EIT FOV, tilted toward the equator as it rose in the Lasco/C1 FOV, and was very symmetric with respect to the equator later in the Lasco C2/C3 FOV. Furthermore, besides the occurrence within the Lasco/C3 FOV, the CME/ICME deflection does exist beyond the near-Sun space. On the basis of statistical analyses of interplanetary scintillation observations, *Wei* [1988] and *Wei and Dryer* [1991] found that the solar-flare-generated shock deflects eastward in the heliospheric equator and equatorward in the heliospheric meridian plane during its interplanetary propagation. This deflection evidence of interplanetary shock aphelion results from joint effects of the (1) spiral interplanetary magnetic field (IMF), (2) westward movement of the heliographic location of a solar flare during the impulsive phase, and (3) heterogenous medium consisting of the fast solar wind from the open corona magnetic field and the slow solar wind astride the heliospheric current sheet [*Hu*, 1998; *Hu and Jia*, 2001]. In addition, the solar source distribution of Earth-encountered halo CMEs is east-west asymmetry [*Wang et al.*, 2002; *Zhang et al.*, 2003]. Some eastern limb CMEs hit the Earth [*Zhang et al.*, 2003], and conversely some disk CMEs missed the Earth [*Schwenn et al.*, 2005]. According to an ICME's kinematic model [*Wang et al.*, 2004], ICMEs could be deflected as much as several tens of degrees during its propagation by the background solar wind and spiral IMF; a fast CME will be blocked by the background solar wind ahead and deflected to the east; a slow CME will be pushed by the following background solar wind and deviated to the west. The existence of ICME deflection is obviously implied from the evidence of indirect observations about the correlations between the near-Sun CME and near-Earth ICME. However, direct observations covering the entire interplanetary space have only been available since the launching of SMEI and STEREO in the twenty-first century. Most of the current spaceborne observations are still heavily concentrated to the 30 solar radii by remote sensing, and the geospace by in situ detecting. As interplanetary observation data is relatively small, numerical simulations are necessary and significant for understanding the whole of interplanetary dynamics, including the deflection effect. *Xiong et al.* [2006b] proposed that (1) the OC between a preceding MC and a following shock results in the simultaneous opposite deflections of the MC body and shock aphelion; (2) an appropriate angular difference between the initial eruptions of an MC and an overtaking shock leads to the maximum deflection of the MC body; and (3) the larger the shock intensity, the greater the deflection angle. As a straightforward analogy to the MC-shock OC [*Xiong et al.*, 2006b], the interplanetary deflection can be also expected for the MC-MC OC. As a result of collision of one MC with either a shock or another MC, the deflection can be ascribed to the interaction between the different interplanetary disturbances. In contrast to our models, the previous deflection models [e.g., *Hu*, 1998; *Hu and Jia*, 2001; *Wang et al.*, 2004] are caused by the interaction between the ambient solar wind and an interplanetary disturbance.

[5] The conjecture about the interplanetary deflection from the MC-MC OC is investigated in this paper. In addition, a simplified circumstance of MC-MC DC, excluding the deflection effect, has already been studied by *Xiong et al.* [2007]. The following conclusions are revealed from the MC-MC DC [*Xiong et al.*, 2007]: (1) when the accumulated magnetic elasticity can balance the external colliding, the compressibility of double MCs reaches its maximum; (2) this cutoff limit of compressibility mainly decides the maximally available geoeffectiveness of double MCs, because geoeffectiveness enhancement of MCs' interacting is ascribed to compression; (3) the magnetic elasticity, magnetic helicity of each MC, and compression between each other are the key physical factors for the formation, propagation, evolution, and resulting geoeffectiveness of interplanetary double MCs. Here the study of MC-MC OC is a more reasonable extension of that of MC-MC DC [*Xiong et al.*, 2007]. Thus two issues are naturally raised: (1) What is the difference between the MC-MC DC and MC-MC OC in terms of the interplanetary dynamics and ensuing geoeffectiveness? (2) Does such a deflection effect caused by the MC-MC OC play a significant or negligible role during interaction process? The answers to these questions are explored by a 2.5-dimensional (2.5-D) numerical model in an ideal MHD process.

[6] The present work targets the OC between two MCs as a logical continuation in a series of studies for the interplanetary compound structures [*Xiong et al.*, 2005, 2006a, 2006b, 2007; *Xiong*, 2007]. We give the numerical MHD model in section 2, describe the dynamics and geoeffectiveness of two typical cases of double MCs in section 3, analyze the roles of eruption interval in section 4, angular difference in section 5, and collision intensity in section 6 for two MCs interacting, and summarize the paper in section 7.

2. Numerical MHD Model

[7] The dynamics and geoeffectiveness of interplanetary compound structures have already been numerically investigated by our effective numerical model [*Xiong et al.*, 2006a, 2006b, 2007; *Xiong*, 2007]. This model quantitatively relates the output of solar disturbances at $25 R_s$ to the interplanetary parameters and geomagnetic storm at 1 AU, thus establishing a cause-and-effect transporting chain for a solar-terrestrial physical process. The concrete implementation of this numerical model consists of two steps: (1) the numerical MHD simulation of interplanetary disturbance propagation, and (2) using the Burton empirical formula for the solar wind-magnetosphere-ionosphere coupling to evaluate the geomagnetic storm index *Dst* [*Burton et al.*, 1975]. The detailed description of the numerical model, including the numerical algorithm, computational grid layout, ambient solar wind, is given by *Xiong et al.* [2006a].

[8] An incidental MC, radially launched from the solar surface, is characterized by several parameters: the emergence speed v_{mc}, latitude θ_{mc}, and time t_{mc}, et al. The following MC2's emergence latitude θ_{mc2} is included for

Table 1. Assortment of Simulation Cases of an Individual MC

Group	Case	v_{mc} (10^2 km/s)	Comment
IPM	P_1	4	individual-preceding MC ($H_{mc} = 1$)
IFM	$F_1, F_2, F_3,$	4.5, 5, 6,	individual-following MC ($H_{mc} = -1$)
	$F_4, F_5, F_6,$	7, 8, 9,	
	F_7, F_8, F_9	10, 11, 12	

parametric study in contrast to the DC along the helio-spheric equator [*Xiong et al.*, 2007]. Both the MCs are consequently injected into the simulation domain through a particular modification of the inner boundary condition at 25 R_s [*Vandas et al.*, 1995; *Xiong et al.*, 2006a]. The DC and OC in the interplanetary medium correspond to $\theta_{mc2} = 0°$ and $\theta_{mc2} \neq 0°$, since the preceding MC1 emerges from the equator, $\theta_{mc1} = 0°$. Moreover, the MC2-driven shock in all of our simulation cases is faster than the local magnetosonic speed at any time in order to prevent weak shock dissipation in the MC body of low plasma β.

3. MC1-MC2 Interaction

[9] All 34 cases of double MCs' interacting are assembled into three groups in Table 2, with 10 cases of an individual MC in two groups from Table 1 for comparison. In Table 2, the helicity of one MC $H_{mc1} = 1$ is opposite to that of the other MC $H_{mc2} = -1$, because this specific helicity combination corresponds to the maximally available geoeffectiveness [*Xiong et al.*, 2007]. Groups of an individual-preceding MC (IPM), an individual-following MC (IFM), an eruption-interval dependence (EID), an angular-difference dependence (ADD), and a collision-intensity dependence (CID) are studied, with case E_2 shared by Groups EID, ADD, and CID. The slow MC1 of $v_{mc1} = 400$ km/s, $H_{mc1} = 1$, $\theta_{mc1} = 0°$, and $t_{mc1} = 0$ hour is chased and pounded by a fast MC2 of various parameters. Here the parametric studies of double MCs cover a wide spectrum of $t_{mc2} = 10.2 \sim 44.1$ hours in group EID, $\theta_{mc2} = 0° \sim 50°$ in group ADD, and $v_{mc2} = 450 \sim 1200$ km/s in group CID. Moreover, by adjusting Dt ($Dt = t_{mc1} - t_{mc2}$, $t_{mc1} = 0$ hour), the initiation delay between the two MC emergences in group EID, an interplanetary compound stream consisting of double MCs may reach a different evolutionary stage when it arrives at 1 AU. The t_{mc2} is prescribed to be 12.2 hours in groups ADD and CID for the full development of double MCs' interacting within 1 AU. In the following we address case E_1 of 30.1 hours and case E_2 of 12.2 hours in group EID, which are typical examples of double MCs in the early and late evolutionary stages.

3.1. Case E_1

[10] Figures 1–4 show the consequent behavior of MC1-MC2 interaction of case E_1 with the eruption speed $v_{mc1} = 400$ km/s, $v_{mc2} = 600$ km/s, and the initiation delay $t_{mc2} = 30.1$ hours. The magnetic field lines, of which two are enclosed with white solid lines marking the boundaries of MC1 and MC2, are superimposed on each image of Figures 1–3. Two radial profiles, one through the equator (noted by Lat. = 0°), the other through 4.5° southward (white dashed lines in Figures 1–3, noted by Lat. = 4.5°S), are plotted in Figure 4. The magnitude B of the magnetic field in the radial profile of Figures 1a–1c is presented by subtracting its initial value $B|_{t=0}$ of ambient equilibrium. The coupling of two MCs could be considered as a comprehensive interaction between two systems, each composed of an MC body and its driven shock. The MC2-driven shock and MC2 body are successively involved in the interaction with the MC1 body. The MC2-driven shock catches up with the MC1 body tail at 48 hours, as seen in Figures 2a and 4d. Across the shock front, impending collision is influenced by the abrupt jump of radial speed v_r from 430 to 650 km/s. From then on, both MCs are coupled with each other to form an interplanetary compound stream of double MCs [*Wang et al.*, 2003a; *Dasso et al.*, 2009]. At 57 hours, the marching MC2-driven shock front behaves as a steep speed jump at MC1's rear part (Figures 2b and 4e), just downstream from which the magnetic magnitude B (Figures 1b and 4b) and fast magnetosonic mode speed c_f (Figures 3b and 4h) are locally enhanced. Because of the large initial delay $t_{mc2} = 30.1$ hours, only the rear half of the MC1 body is swept and compressed by the MC2-driven shock within 1 AU (Figures 2c and 4f).

[11] The in situ observation along Lat. = 4.5°S by a hypothetical spacecraft at the Lagrangian point (L1) is shown in Figure 5. The boundary and core of each MC are identified as dashed and solid lines, respectively. The rear half of the MC1 body is significantly gripped by the penetration of the MC2-driven shock at the MC1 core and the push of the MC2 body upon the MC1 tail. The duration of MC1's rear half (9 hours) is much less than that of MC1's anterior half (16 hours). The dawn-dusk electric field VB_z is swiftly intensified from 0 at 73 hours to -13 mV/m at 76 hours. Because the orientation of the magnetic field within the double flux rope structure is north-south-south-north, the superposition of three individual southward B_s regions from the MC1, IMF, and MC2 behaves as a long-lived geoeffective solar wind flow from 73 to 93 hours

Table 2. Assortment of Simulation Cases of Double MCs[a]

Group	Case	v_{mc2} (10^2 km/s)	θ_{mc2} (deg)	t_{mc2} (hour)	Comment
EID	$E_1, E_2, E_3, E_4,$	6	10	30.1, 12.2, 44.1, 42.1,	eruption-interval
	$E_5, E_6, E_7, E_8,$			40.2, 37.2, 35.1, 33.1,	dependence
	$E_9, E_{10}, E_{11}, E_{12},$			31.5, 28.2, 25.1, 22.1,	
	$E_{13}, E_{14}, E_{15}, E_{16}$			20.1, 17.1, 15.1, 10.2	
ADD	$A_1, A_2, A_3, E_2,$	6	0, 3, 5, 10, 15, 20,	12.2	angular-difference
	$A_4, A_5, A_6, A_7,$		25, 30, 40, 45, 50		dependence
	A_8, A_9, A_{10}				
CID	$C_1, C_2, E_2, C_3,$	4.5, 5, 6, 7,	10	12.2	collision-intensity
	C_4, C_5, C_6, C_7, C_8	8, 9, 10, 11, 12			dependence

[a]Note that $v_{mc1} = 400$ km/s, $\theta_{mc1} = 0°$, $t_{mc1} = 0$ hour, $H_{mc1} = 1$, and $H_{mc2} = -1$ for all 34 cases.

Figure 1. Evolution of an MC2 overtaking an MC1 for case E_1, with magnetic field magnitude B at (a) 48 hours, (b) 57 hours, and (c) 72 hours. The white solid line denotes the MC boundary. The white radial dashed line is along the latitude of 4.5°S. Only the part of domain is adaptively plotted to highlight the double MCs.

(Figure 5d), and results in a one-dip curve of *Dst* with its minimum −234 nT at 87 hours (Figure 5e).

3.2. Case E_2

[12] In case E_2, a much earlier emergence time of the MC2 (t_{mc2} = 12.2 hours) guarantees the full interaction between the two MCs before their arrival at 1 AU. Only the evolution of v_r is given in Figures 6 and 7 to visualize the structure of double MCs. The initial emergence latitudes of MC1 ($\theta_{mc1}|_{t=0}$) and MC2 ($\theta_{mc2}|_{t=0}$) are two important parameters of solar eruption output. The nonzero difference
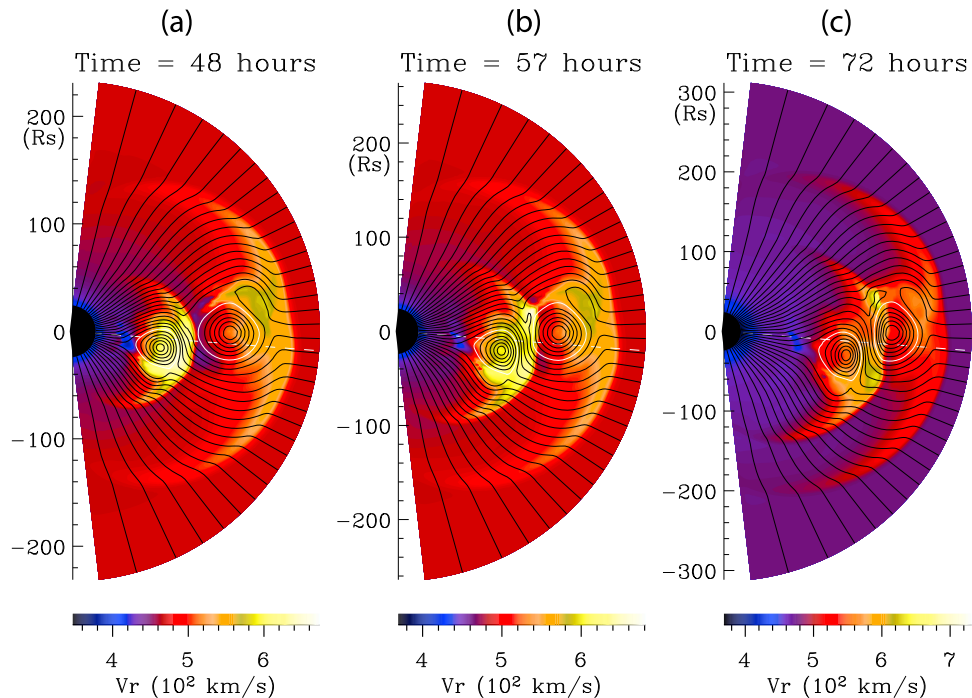

Figure 2. Evolution of an MC2 overtaking an MC1 for case E_1, with radial flow speed v_r at (a) 48 hours, (b) 57 hours, and (c) 72 hours.
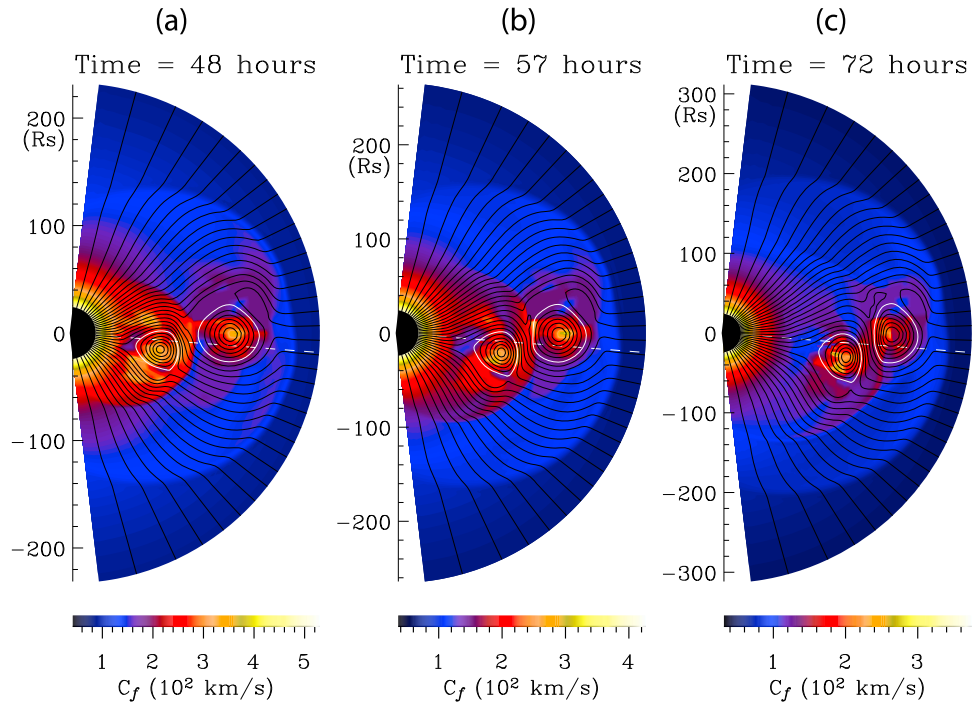
Figure 3. Evolution of an MC2 overtaking an MC1 for case E_1, with radial characteristic speed of fast mode c_f at (a) 48 hours, (b) 57 hours, and (c) 72 hours.

$D\theta|_{t=0}$ ($D\theta|_{t=0} = \theta_{mc2}|_{t=0} - \theta_{mc1}|_{t=0}$) decides a consequent OC in the interplanetary space. The collision between two MCs can be understood by comparison to a billiards game. For one moving rigid ball colliding with another still ball along the radial direction, the response is straightforward in a vacuum: in the DC case, two balls will strictly move along the same radial direction; in the OC case, two balls will oppositely deflect along an angular direction, accompanying
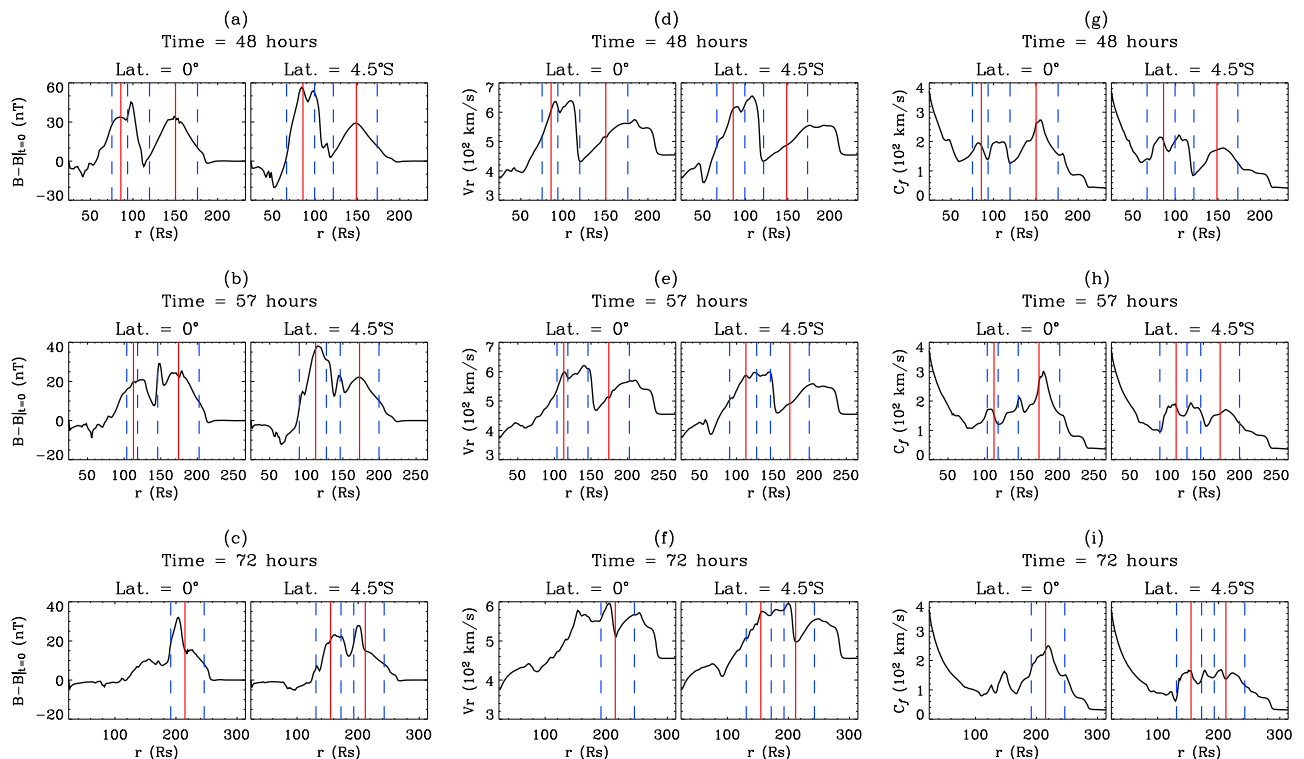
Figure 4. Two radial profiles along the latitudes of $0°$ and $4.5°$S for case E_1. Note that radial profile of B is plotted by subtracting the initial ambient value $B|_{t=0}$. The solid and dashed lines at each profile denote the MC core and boundary, respectively.
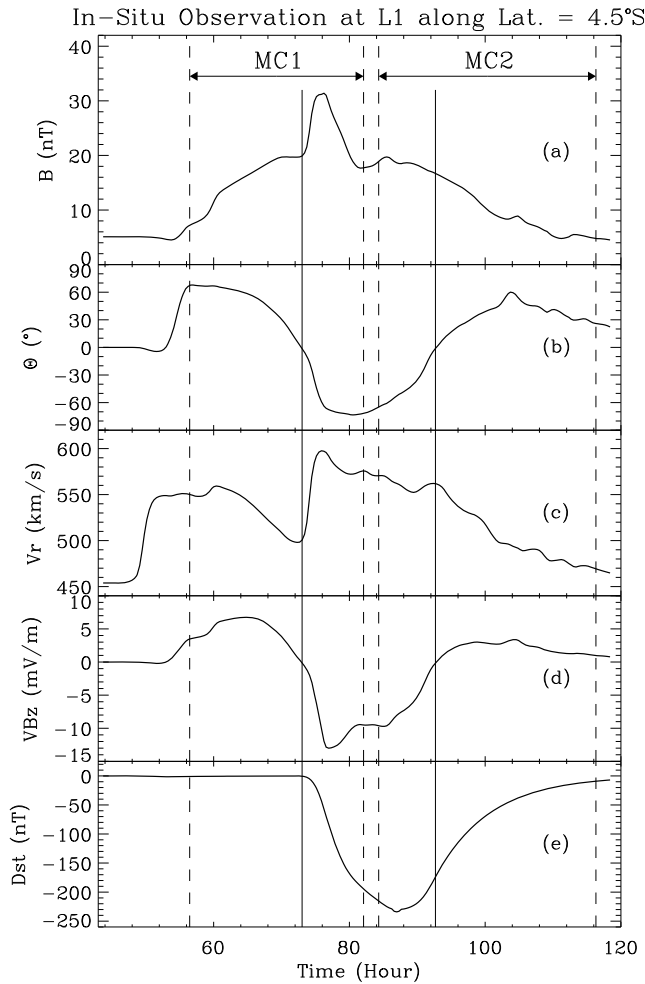
Figure 5. In situ synthetic observations along the latitude of 4.5°S for case E_1. Shown are the (a) magnetic field magnitude B, (b) elevation of magnetic field Θ, (c) radial flow speed v_r, (d) dawn-dusk electric field VB_z, and (e) Dst index. The solid and dashed delimiting lines denote the MC core and boundary, respectively.

their continuous radial movement. The patterns of ball movement contribute to a further quantitative understanding of complex collision between two MCs in the interplanetary medium. The magnetic field lines, frozen in a low β plasma, could be considered as an elastic skeleton embedded in the MC body. The innate magnetic elasticity can efficiently buffer the compression as a result of the colliding of a following MC2 against a leading MC1 [*Xiong et al.*, 2007]. When every MC becomes increasingly stiff, the compression reaches its asymptotic degree. The compressibility effect should be included for the quantitative investigation of deflection effect as a result of OC. Such a task should use numerical MHD simulation, as we demonstrate in this paper. The direction of main compression within the double MCs is parallel/oblique to the radial direction for the DC/OC. For the DC already discussed by *Xiong et al.* [2007], the compression strictly persists along the heliospheric equator and the compressed magnetic flux within the MC body almost points to the south. Therefore, the DC case is very efficient to enhance the geoeffectiveness. The

fast MC2 body continuously strikes the slow MC1 tail, until the MC2 speed is lower than the MC1 speed after momentum transfer. Such MC2 body pushing prevents magnetic field lines in the MC1, previously compressed by MC2-driven shock, from being restored, when the MC2-driven shock completely passes through the MC1 body. For the OC, the compression occurs along one side of each MC. For an example, the MC2 body is faced with the MC1 body from its left side and the ambient solar wind from its right side. Because of the MC1's blocking, the MC2 suffers the compression from its left side. Such an angular pressure imbalance leads to the MC2's right deflection. Simultaneously, the MC1 deflects leftward for the same reason. The opposite deflections, separating double MCs, greatly relieve the intensity of the OC. Therefore, the angular freedom for each MC is an extra factor in efficiently buffering the compression. This angular deflection, absent for the DC case [*Xiong et al.*, 2007], is explored for the OC case here. The IMF lines within the latitude difference ($D\theta|_{t=0} = 10°$ in this case) of two MC eruptions are first draped and then compressed between the MC1 tail and MC2 head. At 22 hours, the left flank of the MC2-driven shock enters the MC1 core (Figures 6a and 7a). Because of very low β in the MC1 medium, the left flank of the shock front in the MC1 body propagates much faster than the right one in the ambient solar wind. The MC1 body is compressed by the MC2-driven shock along its normal. The advance of the MC2-driven shock accompanies a drastic jump of local speed in the MC1 medium. The MC2 body obliquely chases the MC1 body and then grazes the MC1's right boundary. During this process, the momentum is gradually transferred from the following MC2 to the preceding MC1. The location of the most violent interaction within the double MCs, characterized by the greatest compression of local magnetic flux, gradually shifts from the MC1's rear half (Figures 6a and 7a) to the MC1's anterior half (Figures 6b and 7b), and is finally within the MC1-driven sheath (Figures 6c and 7c). The compound stream of double MCs reaches a relatively stable state at 57 hours (Figures 6c and 7c) when the MC2-driven shock ultimately merges with the MC1-driven shock into a stronger compound one.

[13] The time sequence of synthetic measurement at L1 for case E_2 is shown in Figure 8. The speed v_r monotonically decreases from the MC1's head to the MC2's tail (Figure 8c). The magnetic elasticity of southward magnetic flux takes a recovering effect against the previous compression, as the MC2-driven shock continuously moves forward in the MC1 body. As the compression of the MC1's rear half is largely relieved, the duration of geoeffective solar wind flow is prolonged from 20 hours in case E_1 to 31 hours in case E_2. Owing to the OC, the MC1 deflects northward, and the MC2 deviates southward. Largely reduced is the total southward magnetic flux passing through Lat. = 4.5°S. The opposite deflection of the two MCs together with the above mentioned mitigated compression cause a significant increase of Dst from −234 to −121 nT.

[14] The evolution of various physical parameters for each MC in case E_2 is shown in Figure 9. The MC1 is accelerated and the MC2 is decelerated, as seen in Figure 9a. The MC1 begins to deflect northward at 28 hours, 16 hours later than the MC2's southward deflection (Figure 9b). The deflections of both MC1 and MC2 gradually approach an
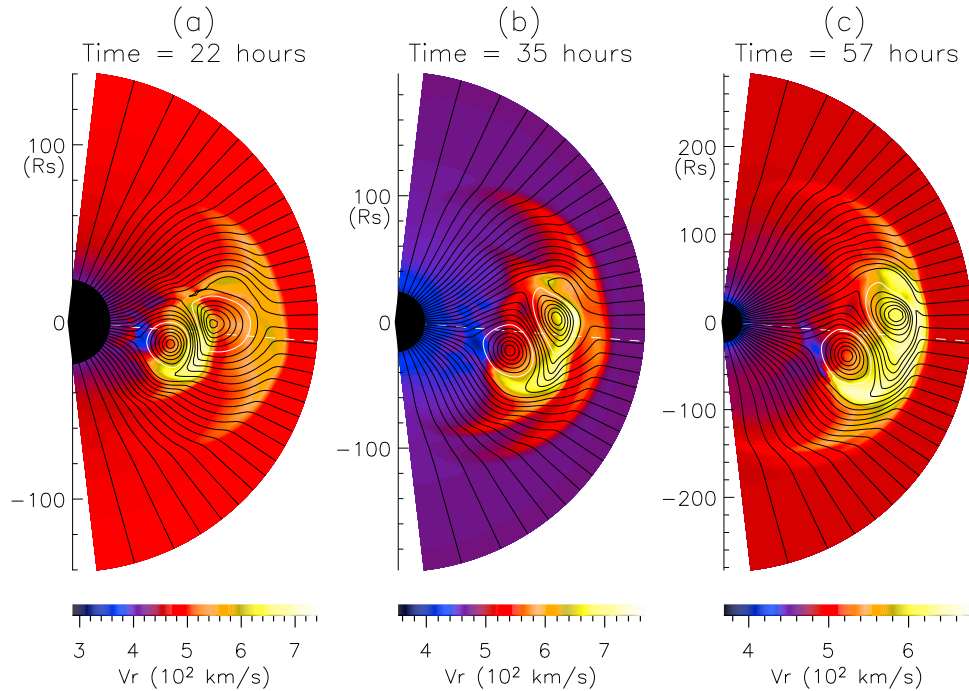
**Figure 6.** Evolution of an MC2 overtaking an MC1 for case E_2, with radial flow speed v_r.

asymptotic values $\delta\theta_{mc1} = -3°$ and $\delta\theta_{mc2} = 6.3°$, respectively. Last, after being pushed aside, the MC1 and MC2 propagate along the latitudes of $\theta_{mc1} = 3°N$ and $\theta_{mc2} = 16.3°S$, respectively. Obviously, the MC2 undergoes a larger deflection than the MC1. Because of the deflection, the distance d between the two MC cores is highly increased in contrast to an uncoupling case (Figure 9c). For an individual MC, the higher the MC speed is, the greater the compression between the MC body and its front ambient solar wind, and the smaller the MC's cross-section area A_{mc}. For an OC case of double MCs, A_{mc} depends on one more compression factor, interaction between two MCs. With the increased speed, the MC1 suffers larger compression from its front ambient solar wind. The MC2's trailing pounding the MC1 compresses the MC1 body. Therefore, the MC1 area A_{mc1} is smaller than its corresponding isolated case (Figure 9d), which is consistent with the DC case [*Xiong et al.*, 2007]. However, the MC2 area A_{mc2} for the OC (Figure 9e) is quite contrary to that for the DC [cf. *Xiong et al.*, 2007, Figure 5d]. The inconsistency is ascribed to the deflection in the OC. For the DC, the compression of MC2 chiefly exists between the MC1 tail and the MC2 head. The persistent blocking of the MC1 body causes the MC2 area shrinkage. For the OC, the MC2 senses the compression from two aspects: (1) the front solar wind and (2) the sideward MC1 body. The MC2 slowdown tends to enhance A_{mc2}, which indicates the mitigated compression between the MC2 body and the solar wind. The blocking of the MC1 body at MC2's left tends to reduce A_{mc2}. As the MC2 deflects sideward, the former factor of the front solar wind contributes more to A_{mc2}, and the latter factor of the sideward MC1 body contributes less. The integration of both competing factors determines the increase or decrease of A_{mc2} in contrast to its corresponding individual MC case. As for the current case E_2, A_{mc2} is increased.

3.3. Latitudinal Distribution of Geoeffectiveness

[15] It has been substantiated from both observation data analyses [e.g., *Burlaga et al.*, 1987; *Wang et al.*, 2003a; *Farrugia et al.*, 2006; *Dasso et al.*, 2009] and numerical simulations [e.g., *Xiong et al.*, 2006a, 2006b, 2007; *Xiong*, 2007] that multiple ICME interactions can significantly enhance the geoeffectiveness at 1 AU. The near-equator latitudinal distribution of *Dst* index is plotted in Figure 10. Since an individual MC would propagate radially through the interplanetary space, the MC core passage corresponds to the strongest geomagnetic storm in a one-dip latitudinal distribution of geoeffectiveness. The strongest geoeffectiveness is -103 nT at $0°$ for an isolated MC1 event (case P_1) and -140 nT at $10°S$ for an isolated MC2 event (case F_3). The coupling of two MCs obviously aggravates the geoeffectiveness. For case E_1, the geoeffectiveness of the two MCs is overlapped, so that the $\theta - Dst$ curve looks like a single dip with its minimum -262 nT at $9°S$. For case E_2, the initial delay between the two MCs is short ($t_{mc2} = 12.2$ hours), the double MCs experience sufficient evolution, the accumulated deflection angle becomes very pronounced, the latitudinal distance between the two MCs becomes large, and the geoeffectiveness of the two MCs is thus separated; hence the $\theta - Dst$ curve behaves like two local dips with their local minima of -200 nT at $15°S$ and -145 nT at $1.5°N$. As the compound stream at 1 AU formed by the two MCs' coupling evolves from case E_1 to E_2, its geoeffectiveness is significantly diffused along the latitude with the intensity largely reduced.

[16] The interplanetary dynamics and resulting geoeffectiveness of the double MCs is a complex system involving multiple independent variables. The parametric studies of eruption-interval dependence (EID), angular-difference dependence (ADD), and collision-intensity dependence (CID) are further explored below to continue the preliminary
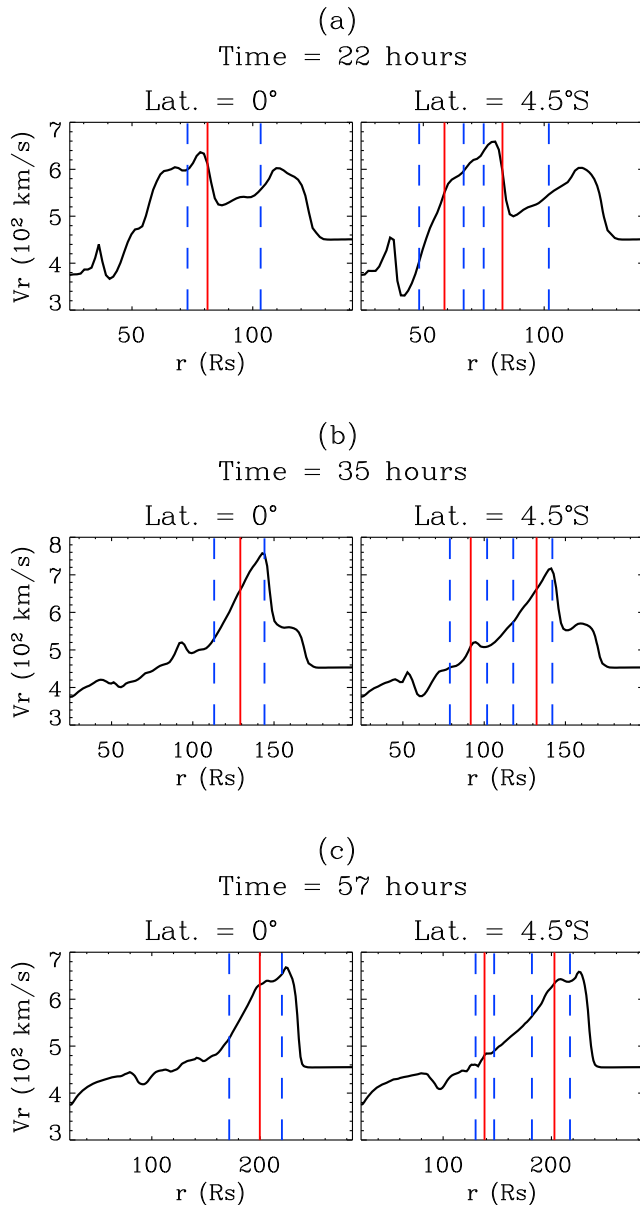
Figure 7. Two radial profiles along the latitudes of 0° and 4.5°S for case E_2.

efforts for the cases E_1, E_2 of double MCs, and the cases P_1, F_3 of a single MC. In sections 4, 5, and 6, the geoeffectiveness of double MCs is described by a scalar of minimum Dst along its latitudinal distribution.

4. Eruption-Interval Dependence

[17] The results of eruption-interval dependence is elucidated in Figure 11. The transfer of momentum from the fast MC2 to the slow MC1 leads to shortening of the Sun-Earth transient time TT_{mc1} and lengthening of TT_{mc2} (Figure 11a). As the initial eruption delay ($t_{mc2} - t_{mc1}$) is shortened, the deflection of each MC exhibits an asymptotic behavior (Figure 11b). When t_{mc2} is reduced from 33.1 to 22.1 hours, and then to 10.2 hours, the MC1 deflection angle $|\delta\theta_{mc1}|$ is increased from 0.2° to 0.7°, and then to 3.3°;

the MC2 deflection angle $|\delta\theta_{mc2}|$ is enhanced from 1.2° to 2.7°, and then to 6.9°; the total deflection angle $\Delta\theta$ ($\Delta\theta = |\delta\theta_{mc1}| + |\delta\theta_{mc2}|$) is changed from 1.4° to 3.4°, and then to 10.2°. These deflection ratios of $|\delta\theta_{mc1}| : |\delta\theta_{mc2}|$ at $t_{mc2} = 33.1$, 22.1, and 10.2 hours correspond to 0.17, 0.26, and 0.48, respectively. Obviously, the MC2 occupies a much bigger share of the total deflection angle $\Delta\theta$. This latitudinal deflection is manifested in the distance d between the cores of MC1 and MC2 at 1 AU (Figure 11d). At the beginning, the magnetic field lines in the MC1 rear half are too vulnerable to resist the MC2's pounding, so the temporarily enhanced compression leads to d decrease. As interpreted in section 3.2, when the most intensely interacting region in the double MCs is shifted from the MC1's rear half, the magnetic elasticity, being passively quenched at the earlier time by the MC2-driven shock, begins to actively bounce to push the two MCs apart. Then the d is steadily increased. Hence the minimum d of 63 R_s exists in an intermediate platform of $t_{mc2} = 22 \sim 28$ hours. Between this zone of $t_{mc2} = 22 \sim 28$ hours, the double MCs suffer the strongest compression, the MC1's cross-section area A_{mc1} is compressed to its minimum $2.4 \times 10^3 R_s^2$ at $t_{mc2} = 22$ hours (Figure 11e), and Dst reaches a minimum of -270 nT at $t_{mc2} = 28$ hours (Figure 11f). When $t_{mc2} \leq 22$ hours, the magnetic
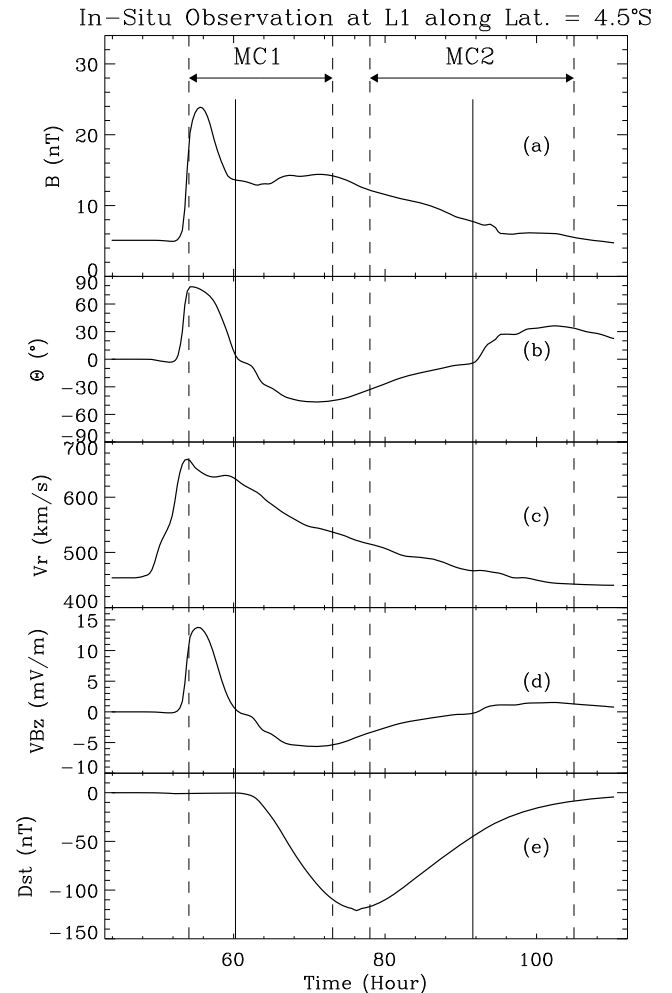
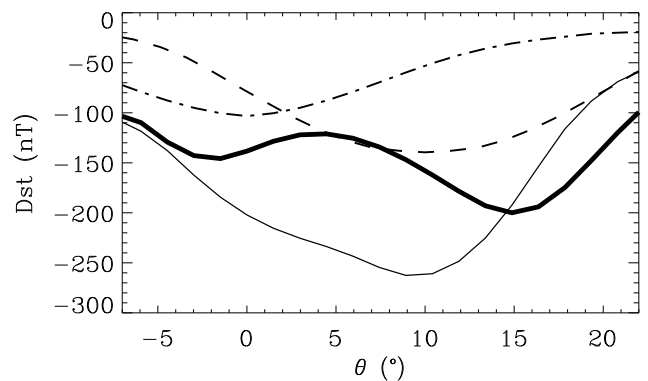**Figure 8.** In situ synthetic observations along the latitude of 4.5°S for case E_2.
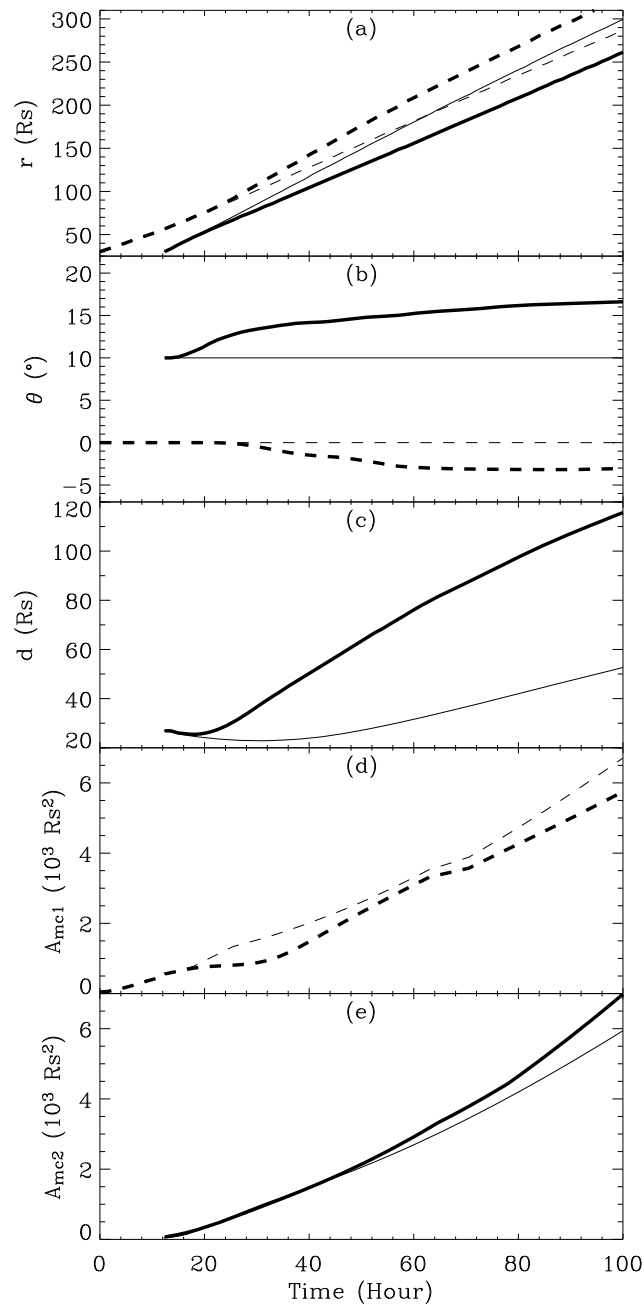
Figure 9. Time dependence of MC parameters: (a) radial distance of MC core r, (b) latitude of MC core θ, (c) distance between both MC cores d, (d) MC1 cross-section area A_{mc1}, and (e) MC2 cross-section area A_{mc2}. In Figures 9a, 9b, 9d, and 9e the thick dashed and solid lines denote the preceding MC1 and following MC2 in case E_2, superimposed with the thin lines for the corresponding individual MC cases for contrast. In Figure 9c the thick and thin lines represent the coupling and noncoupling conditions between two MCs.
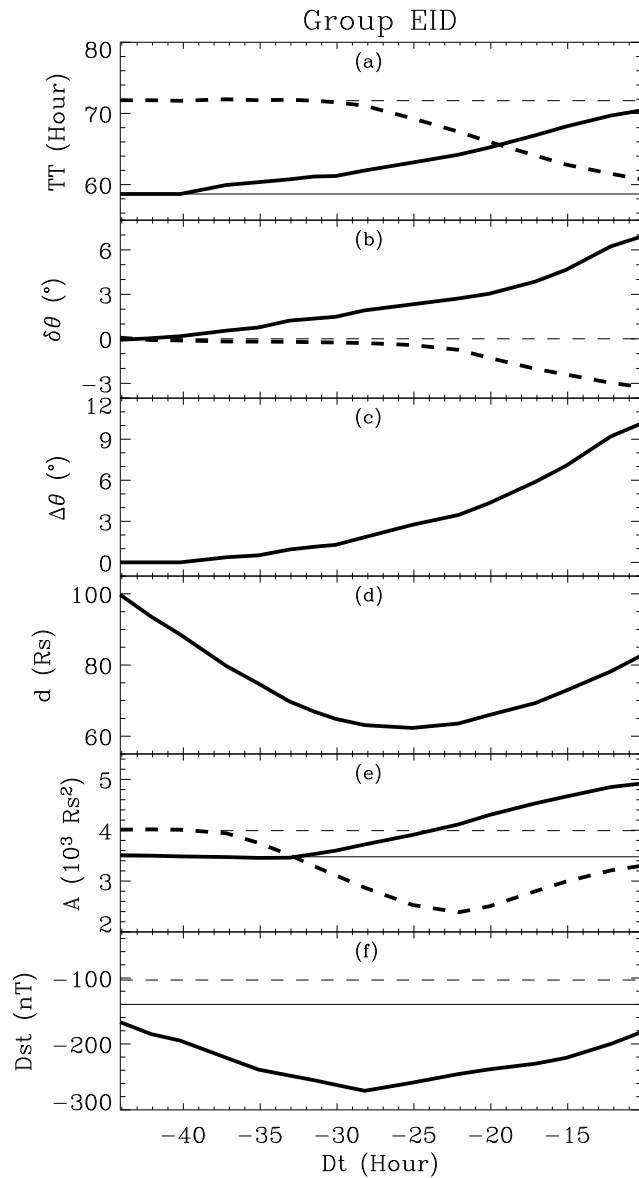
predominance of the MC2's momentum loss over the MC1's blocking is responsible for the monotonic increase of A_{mc2} between $Dt = -32 \sim -10$ hours. These behaviors of the OC case are essentially different from those of the DC case [*Xiong et al.*, 2007]. For the DC case without the deflection effect, the persistent following of the MC2 body at the MC1 tail can inhibit the MC1 body from re-expanding, so the *Dst* can be roughly maintained at a constant, given that the initial delay t_{mc2} is smaller than a certain threshold [cf. *Xiong et al.*, 2007, Figure 9]. The perpetual balance between the external compression and innate elasticity for the DC case is out of equilibrium for the OC case under a new circumstance of angular deflection. Moreover, the external compression could be largely offset by the deflection. Therefore, the OC case is generally weaker for geoeffectiveness than its corresponding DC case, and the strongest geoeffectiveness for the OC case can only be achieved at a certain initial delay between two MC eruptions.

5. Angular-Difference Dependence

[18] The angular-difference dependence is shown in Figure 12. The initial latitudinal difference of $D\theta|_{t=0} = \theta_{mc2}|_{t=0} - \theta_{mc1}|_{t=0}$ for solar output decides the oblique degree of interplanetary collision between two MCs. Corresponding to the nonexistence of deflection, $D\theta|_{t=0} = 0°$ is due to the symmetrical condition, which was thoroughly addressed by *Xiong et al.* [2007]. When $D\theta|_{t=0}$ is too large, the OC effect will be significantly mitigated, and the consequent deflection will be obviously weak. An appropriate $D\theta|_{t=0}$ corresponds to the maximum deflection of OC cases of double MCs, very similar to the known conclusion for the OC case of "a shock overtaking an MC" [*Xiong et al.*, 2006b]. At $D\theta|_{t=0} = 15°$, the total deflection angle $\Delta\theta$ reaches its maximum $12.2°$ with $\delta\theta_{mc1} = -3.8°$ and $\delta\theta_{mc2} = 8.4°$. The $|\delta\theta_{mc2}|$ is generally larger than the $|\delta\theta_{mc1}|$, but it does not match the case of $D\theta|_{t=0} > 40°$. When $D\theta|_{t=0} > 40°$, the two MCs are so widely separated that the interaction is virtually ascribed to the coupling of the MC1 body and the MC2-driven shock. Such indirect interaction between the two MC bodies to transfer momentum clarifies $|\delta\theta_{mc1}| > |\delta\theta_{mc2}|$ for $D\theta|_{t=0} = 40° \sim 50°$ (Figure 12b) and the A_{mc2} decrease for $D\theta|_{t=0} = 20° \sim 50°$ (Figure 12e).

elasticity restoration and angular deflection lead to the increasingly weak compression between two clouds and a consequent increase in A_{mc1}. In addition, according to the reasons given in section 3.2 for the A_{mc2} variance, the

Figure 10. Comparison of latitudinal distribution of *Dst* index among the compound stream cases E_1 (thin solid) and E_2 (thick solid) and corresponding individual-MC cases P_1 (dash-dotted) and F_3 (dashed).
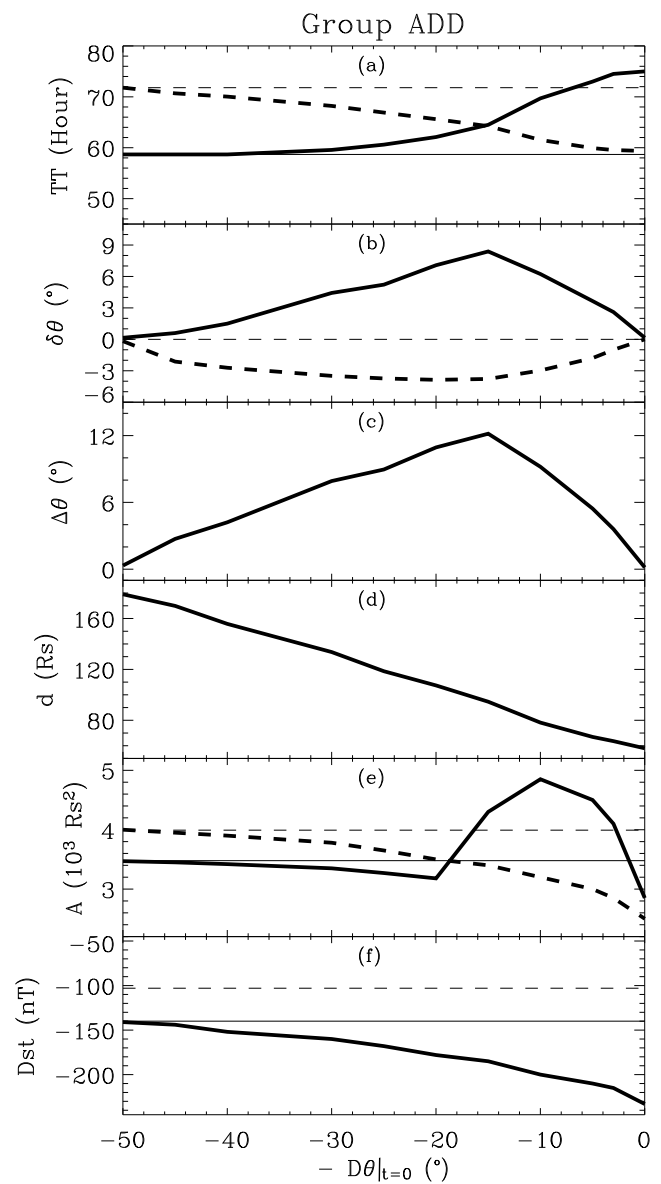
Group EID

the distance d at 1 AU (Figure 12d). As $D\theta|_{t=0}$ decreases, the Dst, being steadily reduced with a steeper slope, changes from -140 nT at $D\theta|_{t=0} = 50°$ to -230 nT at $D\theta|_{t=0} = 0°$. The less the deflection effect, the more compact the multiple interplanetary geoeffective triggers and the more violent the ensuing geomagnetic storm.

6. Collision-Intensity Dependence

[19] Figure 13 displays the collision-intensity dependence. The variance of v_{mc2} corresponds to a different individual MC2 event. As v_{mc2} increases, both TT_{mc1} and TT_{mc2} decrease. However, the decreased TT_{mc2} in the case of double MCs is still larger than its corresponding individual MC case (Figure 13a). The influence of the OC intensity can be described by the v_{mc2} in some senses. As an

Group ADD

Figure 11. Dependence of the compound stream parameters at 1 AU on the MC1-MC2 eruption delay Dt ($Dt = t_{mc1} - t_{mc2}$) in group EID: the (a) Sun-Earth transient time TT, (b) deflection angle of each MC $\delta\theta$, (c) total deflection angle of double MCs $\Delta\theta$ ($\Delta\theta = |\delta\theta_{mc1}| + |\delta\theta_{mc2}|$), (d) distance between the two MC cores d when the MC1 core reaches 1 AU, (e) cross-section area of each MC A, and (f) Dst index. The thick dashed/solid lines in Figures 11a, 11b, 11e, and 11f refer to the occasion of MC1/MC2 core reaching 1 AU. The thin dashed and solid lines in Figures 11a, 11b, 11e, and 11f denote the isolated MC1 and MC2 events for comparison.

With respect to the A_{mc2} variance for $D\theta|_{t=0} \leq 20°$, two competing factors of MC2 momentum loss and MC1 body blocking take effect, as previously interpreted in section 3.2. The dominance of the MC2 momentum loss accounts for the increase between $D\theta|_{t=0} = 10° \sim 20°$; that of the MC1 body blocking elucidates the decrease between $D\theta|_{t=0} = 0° \sim 10°$. The closer the two MCs in the near-Sun position, the smaller

Figure 12. Dependence of the compound stream parameters at 1 AU on the angular difference $-D\theta|_{t=0}$ of the two MC eruptions in group ADD. Here $-D\theta|_{t=0} = -1 \cdot D\theta|_{t=0} = \theta_{mc1}|_{t=0} - \theta_{mc2}|_{t=0}$.
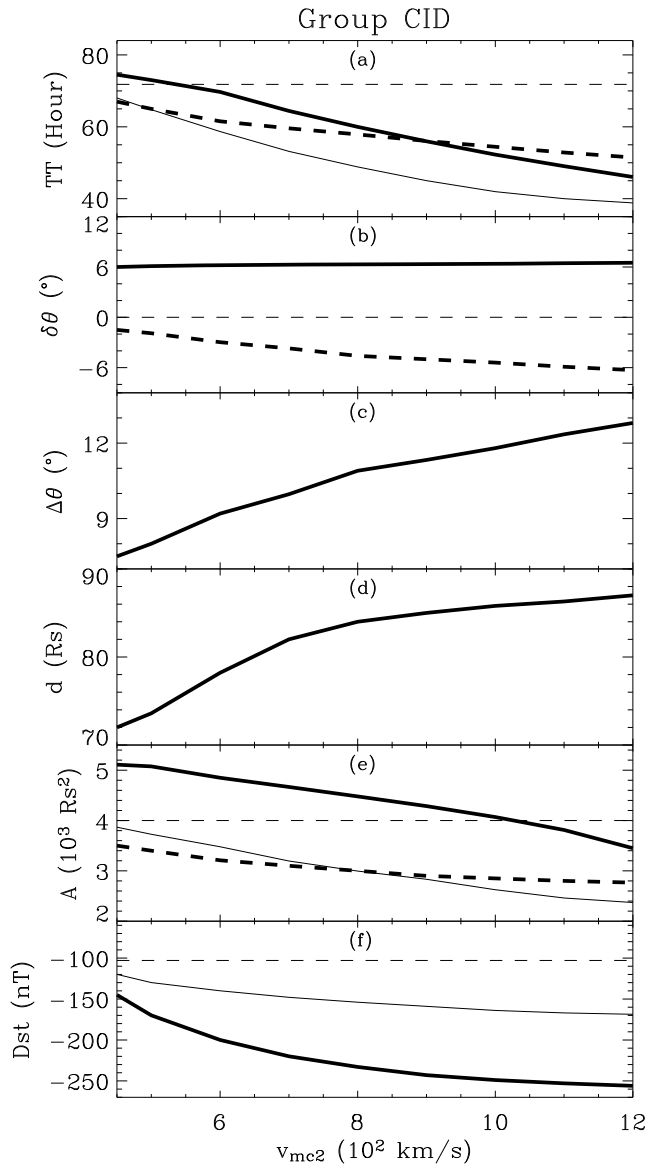
Figure 13. Dependence of the compound stream parameters at 1 AU on the MC2 eruption speed v_{mc2} in group CID.

asymptotic response to the v_{mc2} increase from 450 to 1200 km/s, the geoeffective *Dst* decreases from -145 to -255 nT (Figure 13f), and the total deflection angle $\Delta\theta$ increases from $7.5°$ to $12.8°$ (Figure 13c). The contribution of $\Delta\theta$ almost stems from the MC1 deflection δ_{mc1}, since the MC2 deflection angle δ_{mc2} is nearly constant at $6°$ (Figure 13b). The deflection ratio between the MC1 and MC2 $|\delta\theta_{mc1}|$: $|\delta\theta_{mc2}|$ is 0.3 at $v_{mc2} = 450$ km/s, 0.7 at $v_{mc2} = 800$ km/s, and 1 at $v_{mc2} = 1200$ km/s. Therefore, the cause of intensity aggravation of two MCs' colliding is mainly manifested in the response of the preceding MC1 body. In addition, for the case of $D\theta|_{t=0} = 10°$ in group ADD, the MC2's cross-section area A_{mc2} of a coupled case is larger than that of an isolate case (Figure 12e). Since $D\theta|_{t=0}$ equals $10°$ in group CID, the A_{mc2} behavior is similar for the reason explained in section 5. Furthermore, the more intense the OC between

two MCs, the more violent the compression in the double MCs, and the stronger the accumulated innate magnetic elasticity against the external compression. So the deflection angle $\delta\theta$ (Figure 13b), the distance between the two MC cores d (Figure 13d), and the geoeffective *Dst* (Figure 13f) all exhibit an asymptotic behavior.

7. Conclusions and Summary

[20] The dynamics and geoeffectiveness of interplanetary compound structures such as the complex ejecta [*Xiong et al.*, 2005], MC-shock [*Xiong et al.*, 2006a, 2006b], and MC-MC [*Xiong et al.*, 2007] have been comprehensively investigated during the recent years with our 2.5-D numerical model within an ideal MHD framework. As a logically direct continuation to the DC mode between a preceding MC1 and a following MC2 [*Xiong et al.*, 2007], the OC mode is further explored here to highlight a deflection effect from the parametric studies of eruption-interval dependence, angular-difference dependence, and collision-intensity dependence. The deflection angle for an MC1-MC2 OC in this paper is obviously greater than that for an MC-shock OC addressed by *Xiong et al.* [2006b], as the MC1-MC2 coupling involves a comprehensive interaction among the MC1-driven shock, the MC1 body, the MC2-driven shock, and the MC2 body.

[21] An interplanetary compound stream is formed as a result of interaction between two MCs in the interplanetary space. The direction of main compression within the double MCs is parallel/oblique to the radial direction for the DC/OC. The OC leads to first compress each MC on one side, then push the MC to the other side as a result of angular pressure imbalance. Such a deflection effect for the OC case is essentially absent for the DC case. The deflection angles of MC1 ($|\delta\theta_1|$) and MC2 ($|\delta\theta_2|$) asymptotically approach their corresponding limits, when the two MC-driven shocks are merged into a stronger compound shock. During this process, the geoeffectiveness of double MCs is significantly diffused along the latitudinal distribution, with the intensity largely reduced. An appropriate angular difference between the initial eruptions of two MCs leads to the maximum deflection of $|\delta\theta_1|$ and $|\delta\theta_2|$. A continuous increase of OC intensity can synchronously enhance $|\delta\theta_1|$ and $|\delta\theta_2|$, although its effect becomes less and less obvious. The response of $|\delta\theta_1|$ is far more sensitive than that of $|\delta\theta_2|$. The $|\delta\theta_1|$ is generally far less than the $|\delta\theta_2|$, and the unusual case of $|\delta\theta_1| \simeq |\delta\theta_2|$ only occurs for the extremely intense OC. The opposite deflection between two MCs, together with the inherent magnetic elasticity of each MC, could efficiently buffer the external compression for the interplanetary OC.

[22] The axial variance of an MC is ignored in our model for simplification, so that the geometry of an MC is reduced to be 2.5-D. In reality, both feet of an interplanetary MC is still connected to the solar surface, as substantiated from the evidence of bidirectional electron fluxes along an MC's axis [*Larson et al.*, 1997]. However, for the local analyses of a cross section of an MC, a locally cylindric flux rope has widely been used to approximate the globally curved one, such as the data inversion from the near-Earth in situ observations [*Burlaga et al.*, 1981], the kinematic model of an MC propagation [*Owens et al.*, 2006], and the

numerical simulation of magnetic flux rope dynamics [*Schmidt and Cargill*, 2004; *Xiong et al.*, 2006a]. Hence, our 2.5-D model can well reflect some dynamic characteristics of 3-D MCs to some extent.

[23] An assimilatively integrated study of observation data analyses and numerical simulations is crucial and effective for an in-depth and overall understanding of the Sun-Earth system. As a CME is 3-D by nature, a 2.5-D model has serious limitations in space weather predicting, and a full 3-D numerical model is indispensable to describe realistic observation events [*Feng et al.*, 2007; *Shen et al.*, 2007]. On the one hand, data-driven 3-D models can be tested and improved by using observation data; on the other hand, observations can be better interpreted by using global 3-D models. For instance, demonstrating a good match between synthetic and real STEREO/SECCHI images, *Lugaz et al.* [2009] quantitatively analyzed and well explained the CME events on 24–25 January 2007 by a data-driven 3-D numerical MHD model. Hence, two MCs' interacting in the 2.5-D model in this paper is meaningfully generalized to a 3-D geometry. Such model generalization and then detailed comparison with realistic events are out of contents in this paper and will be addressed in our near future.

[24] In closing, the interaction among multiple CMEs/ICMEs can be a cause of angular deflection during the CME/ICME propagation. Such angular displacement, being nonlinear and irreversible, results in the significant responses of interplanetary dynamics and ensuing geo-effectiveness. Therefore, when successive CMEs from the solar corona are likely to collide with each other obliquely in the interplanetary space, the factor of potential deflection due to the OC should be considered for the geoeffectiveness prediction at 1 AU, as well as the correlation between the near-Sun and the near-Earth observations.

References

Berdichevsky, D. B., I. G. Richardson, R. P. Lepping, and S. F. Martin (2005), On the origin and configuration of the 20 March 2003 interplanetary shock and magnetic cloud at 1 AU, *J. Geophys. Res.*, *110*, A09105, doi:10.1029/2004JA010662.

Burlaga, L. F., E. Sittler, F. Mariani, and R. Schwenn (1981), Magnetic loop behind an interplanetary shock: Voyager, Helios, and IMP 8 observations, *J. Geophys. Res.*, *86*, 6673–6684.

Burlaga, L. F., K. W. Behannon, and L. W. Klein (1987), Compound streams, magnetic clouds, and major geomagnetic storms, *J. Geophys. Res.*, *92*, 5725–5734.

Burlaga, L. F., S. P. Plunkett, and O. C. St. Cyr (2002), Successive CMEs and complex ejecta, *J. Geophys. Res.*, *107*(A10), 1266, doi:10.1029/2001JA000255.

Burton, R. K., R. L. McPherron, and C. T. Russell (1975), An empirical relationship between interplanetary conditions and *Dst*, *J. Geophys. Res.*, *80*, 4204–4214.

Chen, Y., G. Q. Li, and Y. Q. Hu (2006), Force balance analysis of a coronal magnetic flux rope in equilibrium or eruption, *Astrophys. J.*, *649*, 1093–1099.

Chen, Y., Y. Q. Hu, and S. J. Sun (2007), Catastrophic eruption of magnetic flux rope in the corona and solar wind with and without magnetic reconnection, *Astrophys. J.*, *665*, 1421–1427.

Cremades, H., and V. Bothmer (2004), On the three-dimensional configuration of coronal mass ejections, *Astron. Astrophys.*, *422*, 307–322.

Dasso, S., et al. (2009), Linking two consecutive nonmerging magnetic clouds with their solar sources, *J. Geophys. Res.*, *114*, A02109, doi:10.1029/2008JA013102.

Dryer, M. (1994), Interplanetary studies: Propagation of disturbances between the Sun and the magnetosphere, *Space Sci. Rev.*, *67*, 363–419.

Farrugia, C. J., and D. B. Berdichevsky (2004), Evolutionary signatures in complex ejecta and their driven shocks, *Ann. Geophys.*, *22*, 3679–3698.

Farrugia, C. J., V. K. Jordanova, M. F. Thomsen, G. Lu, S. W. H. Cowley, and K. W. Ogilvie (2006), A two-ejecta event associated with a two-step geomagnetic storm, *J. Geophys. Res.*, *111*, A11104, doi:10.1029/2006JA011893.

Feng, X., Y. Zhou, and S. T. Wu (2007), A novel numerical implementation for solar wind modeling by the modified conservation element/solution element method, *Astrophys. J.*, *655*(2), 1110–1126.

Gopalswamy, N. (2002), CME: Propagation and interaction, lecture presented at International Symposium on Solar Activity, Natl. Nat. Sci. Found. of China, Weihai, China.

Gopalswamy, N., S. Yashiro, M. L. Kaiser, R. A. Howard, and J. L. Bougeret (2001), Radio signatures of coronal mass ejection interaction: Coronal mass ejection cannibalism?, *Astrophys. J.*, *548*, L91–L94.

Gopalswamy, N., S. Yashiro, M. L. Kaiser, R. A. Howard, and J.-L. Bougeret (2002), Interplanetary radio emission due to interaction between two coronal mass ejections, *Geophys. Res. Lett.*, *29*(8), 1265, doi:10.1029/2001GL013606.

Gosling, J. T., D. J. McComas, J. L. Phillips, and S. J. Bame (1991), Geomagnetic activity associated with Earth passage of interplanetary shock disturbances and coronal mass ejections, *J. Geophys. Res.*, *96*, 7831–7839.

Hu, Y. Q. (1998), Asymmetric propagation of flare-generated shocks in the heliospheric equatorial plane, *J. Geophys. Res.*, *103*, 14,631–14,642.

Hu, Y. Q., and X. Z. Jia (2001), Interplanetary shock interaction with the heliospheric current sheet and its associated structures, *J. Geophys. Res.*, *106*, 29,299–29,304.

Larson, D. E., et al. (1997), Tracing the topology of the october 18–20, 1995, magnetic cloud with ~0.1 – 10^2 keV electrons, *Geophys. Res. Lett.*, *24*, 1911–1914.

Lepping, R. P., et al. (1997), The Wind magnetic cloud and events of October 18–20, 1995: Interplanetary properties and as triggers for geomagnetic activity, *J. Geophys. Res.*, *102*, 14,049–14,063.

Li, B., and X. Li (2006), Effects of alpha particles on the angular momentum loss from the Sun, *Astron. Astrophys.*, *456*, 359–365.

Li, B., and X. Li (2007), Propagation of non-Wentzel-Kramers-Brillouin Alfvén waves in a multicomponent solar wind with differential ion flow, *Astrophys. J.*, *661*, 1222–1233.

Li, B., and X. Li (2008), Effects of non-WKB Alfvén waves on a multicomponent solar wind with differential ion flow, *Astrophys. J.*, *682*, 667–678.

Li, B., and X. Li (2009), Angular momentum transport in a multicomponent solar wind with differentially flowing, thermally anisotropic ions, *Astron. Astrophys.*, *494*, 361–371.

Li, B., X. Li, Y.-Q. Hu, and S. R. Habbal (2004), A two-dimensional Alfvén wave-driven solar wind model with proton temperature anisotropy, *J. Geophys. Res.*, *109*, A07103, doi:10.1029/2003JA010313.

Li, B., S. R. Habbal, and X. Li (2007), Angular momentum transport and proton-alpha differential streaming in the solar wind, *Astrophys. J.*, *661*, 593–601.

Lugaz, N., W. B. Manchester IV, and T. I. Gombosi (2005), Numerical simulation of the interaction of two coronal mass ejections from Sun to Earth, *Astrophys. J.*, *634*, 651–662.

Lugaz, N., A. Vourlidas, I. I. Roussev, and H. Morgan (2009), Solar-terrestrial simulation in the STEREO era: The 24–25 January 2007 eruptions, *Sol. Phys.*, *256*, 269–284.

MacQueen, R. M., A. J. Hundhausen, and C. W. Conover (1986), The propagation of coronal mass ejection transients, *J. Geophys. Res.*, *91*, 31–38.

Owens, M. J., V. G. Merkin, and P. Riley (2006), A kinematically distorted flux rope model for magnetic clouds, *J. Geophys. Res.*, *111*, A03104, doi:10.1029/2005JA011460.

Richardson, I. G., and H. V. Cane (2004), The fraction of interplanetary coronal mass ejections that are magnetic clouds: Evidence for a solar cycle variation, *Geophys. Res. Lett.*, *31*, L18804, doi:10.1029/2004GL020958.

Schmidt, J. M., and P. J. Cargill (2004), A numerical study of two interacting coronal mass ejections, *Ann. Geophys.*, *22*, 2245–2254.

Schwenn, R., A. Dal Lago, E. Huttunen, and W. D. Gonzalez (2005), The association of coronal mass ejection with their effects near the Earth, *Ann. Geophys.*, 23, 1033–1059.

Shen, F., X. Feng, S. T. Wu, and C. Xiang (2007), Three-dimensional MHD simulation of CMEs in three-dimensional background solar wind with the self-consistent structure on the source surface as input: Numerical simulation of the January 1997 Sun-Earth connection event, *J. Geophys. Res.*, 112, A06109, doi:10.1029/2006JA012164.

Tsurutani, B. T., E. J. Smith, W. D. Gonzalez, F. Tang, and S. I. Akasofu (1988), Origin of interplanetary southward magnetic fields responsible for major magnetic storms near solar maximum (1978–1979), *J. Geophys. Res.*, 93, 8519–8531.

Vandas, M., S. Fischer, M. Dryer, Z. Smith, and T. Detman (1995), Simulation of magnetic cloud propagation in the inner heliosphere in two dimensions: 1. A loop perpendicular to the ecliptic plane, *J. Geophys. Res.*, 100, 12,285–12,292.

Vandas, M., S. Fischer, M. Dryer, Z. Smith, T. Detman, and A. Geranios (1997), MHD simulation of an interaction of a shock wave with a magnetic cloud, *J. Geophys. Res.*, 102, 22,295–22,300.

Wang, Y. M., P. Z. Ye, S. Wang, G. P. Zhou, and J. X. Wang (2002), A statistical study on the geoeffectiveness of Earth-directed coronal mass ejections from March 1997 to December 2000, *J. Geophys. Res.*, 107(A11), 1340, doi:10.1029/2002JA009244.

Wang, Y. M., P. Z. Ye, and S. Wang (2003a), Multiple magnetic clouds: Several examples during March–April 2001, *J. Geophys. Res.*, 108(A10), 1370, doi:10.1029/2003JA009850.

Wang, Y. M., P. Z. Ye, S. Wang, and X. H. Xue (2003b), An interplanetary cause of large geomagnetic storms: Fast forward shock overtaking preceding magnetic cloud, *Geophys. Res. Lett.*, 30(13), 1700, doi:10.1029/2002GL016861.

Wang, Y. M., C. L. Shen, S. Wang, and P. Z. Ye (2004), Deflection of coronal mass ejection in the interplanetary medium, *Sol. Phys.*, 222, 329–343.

Wei, F. S. (1988), Statistic study on asymmetric propagation of flare-associated interplanetary shock waves, *Sci. Sin. Ser. A*, 31, 451–460.

Wei, F. S., and M. Dryer (1991), Propagation of solar flare-associated interplanetary shock waves in the heliospheric meridional plane, *Sol. Phys.*, 132, 373–394.

Wei, F., R. Liu, Q. Fan, and X. Feng (2003), Identification of the magnetic cloud boundary layers, *J. Geophys. Res.*, 108(A6), 1263, doi:10.1029/2002JA009511.

Wei, F., X. Feng, F. Yang, and D. Zhong (2006), A new non-pressure-balanced structure in interplanetary space: Boundary layers of magnetic clouds, *J. Geophys. Res.*, 111, A03102, doi:10.1029/2005JA011272.

Williamson, S. P., D. L. Evans, C. M. A. Neyland, M. S. Leinen, E. J. Weiler, R. E. Waldron, D. Whatley, and J. F. Devine (2001), *National Space Weather Program: The Implementation Plan*, 2nd ed., *FCM-P31-2000*, Off. of the Fed. Coord. for Meteorol. Serv. and Support. Res., Natl. Space Weather Program Counc., Washington, D. C.

Xia, L. D. (2003), Equatorial coronal holes and their relation to the high-speed solar wind streams, Ph.D. dissertation, Georg-August-Univ., Göttingen, Germany.

Xia, L. D., E. Marsch, and W. Curdt (2003), On the outflow in an equatorial coronal hole, *Astron. Astrophys.*, 399, L5–L9.

Xia, L. D., E. Marsch, and K. Wilhelm (2004), On the network structures in solar equatorial coronal holes. Observations of SUMER and MDI on SOHO, *Astron. Astrophys.*, 424, 1025–1037.

Xiong, M. (2007), Numerical MHD simulation of the dynamics and geoeffectiveness of some interplanetary compound structures, Ph.D. dissertation, Univ. of Sci. and Technol. of China, Hefei, China.

Xiong, M., H. N. Zheng, Y. M. Wang, X. R. Fu, S. Wang, and X. K. Dou (2005), A numerical simulation on the solar-terrestrial transit time of successive CMEs during November 4–5, 1998, *Chin. J. Geophys.*, 48, 805–813.

Xiong, M., H. Zheng, Y. Wang, and S. Wang (2006a), Magnetohydrodynamic simulation of the interaction between interplanetary strong shock and magnetic cloud and its consequent geoeffectiveness, *J. Geophys. Res.*, 111, A08105, doi:10.1029/2005JA011593.

Xiong, M., H. Zheng, Y. Wang, and S. Wang (2006b), Magnetohydrodynamic simulation of the interaction between interplanetary strong shock and magnetic cloud and its consequent geoeffectiveness: 2. Oblique collision, *J. Geophys. Res.*, 111, A11102, doi:10.1029/2006JA011901.

Xiong, M., H. Zheng, S. T. Wu, Y. Wang, and S. Wang (2007), Magneto-hydrodynamic simulation of the interaction between two interplanetary magnetic clouds and its consequent geoeffectiveness, *J. Geophys. Res.*, 112, A11103, doi:10.1029/2007JA012320.

Zhang, J., K. P. Dere, R. A. Howard, and V. Bothmer (2003), Identification of solar sources of major geomagnetic storms between 1996 and 2000, *Astrophys. J.*, 582, 520–533.

Zhang, J., K. P. Dere, R. A. Howard, and A. Vourlidas (2004), A study of the kinematic evolution of coronal mass ejections, *Astrophys. J.*, 604, 420–432.

————————————

S. Wang, M. Xiong, and H. Zheng, Chinese Academy of Sciences Key Laboratory for Basic Plasma Physics, School of Earth and Space Sciences, University of Science and Technology of China, Hefei, Anhui 230026, China. (swan@ustc.edu.cn; mxiong@ustc.edu.cn; hue@ustc.edu.cn)